Title: Improving the understanding of cytoneme-mediated morphogen gradients by *in silico* modeling

Authors: Adrián Aguirre-Tamaral[1]* and Isabel Guerrero[1]*

Affiliations: [1]Tissue and Organ Homeostasis, Centro de Biología Molecular "Severo Ochoa" (CSIC-UAM), Nicolás Cabrera 1, Universidad Autónoma de Madrid, Cantoblanco, E-28049 Madrid, Spain.

*Corresponding authors: adrian.aguirre@cbm.csic.es and iguerrero@cbm.csic.es

Abstract: Morphogen gradients are crucial for the development of organisms, but there is still no agreement on the mechanisms involved in their establishment. The biochemical properties of many morphogens prevent their extracellular free diffusion, indicating the need for an active mechanism for transport. The involvement of filopodial structures (cytonemes) has been proposed for morphogen signaling, although a detailed description of the mechanism is pending. Here, we describe the development of an *in silico* model based on the main general features of cytoneme-meditated gradient formation and its implementation into an open software tool we named Cytomorph. We have tested the spatial and temporal adaptability of our model experimentally quantifying Hedgehog (Hh) gradient formation in *Drosophila* and found that Cytomorph is able to reproduce the gradient and explain its scaling between different epithelia. After experimental validation, we studied the predicted impact of a range of features such as length, size, density, dynamics and contact behavior of cytonemes on morphogen distribution. Our results illustrate Cytomorph as an adaptive tool to test and generate hypotheses that are difficult to study experimentally.

Key words: In silico modeling, Cytonemes, Morphogen gradient, Hedgehog signaling.

Introduction

During embryonic development, groups of cells are organized to give rise to tissues and organs. Precise spatio-temporal control of cell-to-cell communication during proliferation, differentiation and three-dimensional cell organization, is needed for proper development. Misregulation of these events is one of the most prevalent causes of diseases such as congenital malformations, cancer and neurological disorders (1). Several signaling molecules act as messengers between cells and are transported from producing to target cells to regulate all these processes. Some of these signal molecules function as morphogens, acting at a distance in a concentration-dependent manner to regulate the differential activation of target genes (2). The distribution of signals to form concentration gradients requires a tight spatiotemporal regulation. However, the cellular mechanisms involved in the transport of the morphogens are still under debate (3).

Modeling has been a useful strategy to explore complex biological processes. Models to explain pattern generation during development have been mainly focused on the description of how, when and where a morphogenetic signal induces a specific cellular response within a particular tissue. Especially relevant were the early works of A. Turing (4) and L. Wolpert (5), who set the foundation of how a precise morphogen distribution could determine cell fates and patterns in a concentration-dependent manner. Subsequently, several works took into account the effect of the production and degradation of morphogens (6–9) and usually their transport was modeled simply by inferring a diffusion mechanism (10). Since the molecular properties of most morphogens impede them to diffuse freely in the extracellular environment a different mechanism for their transport would be required (11). A transport mechanism based on filopodia-like-structures, also called cytonemes, has been proposed for most signaling pathways (12–15): BMP (16,17), Wnt (18,19), EGF (20), FGF (20), Hedgehog (Hh) (21–23) and Notch

(24–27). Furthermore, live imaging in developing tissues (22,23,28–30) has revealed cytoneme dynamics as essential for correct cell signaling.

Cytonemes are actin-based membrane protrusions emanating from morphogen producing and/or receiving cells that deliver or collect morphogen by direct cell-cell membrane contacts (Fig.1). Increasing experimental evidence highlights the implication of cytonemes in short-and long-distance cell communication. In parallel, a few mathematical models centered on different aspects of cytoneme-mediated signaling have also been proposed (reviewed at (31). They focus in characteristics such as, vesicular transport along cytonemes (32,33), cytoneme contact mechanisms (34) or cytoneme guidance towards correct target receiving cell in a 1D system (35).

To date there are also some models concerning the cytoneme-mediated establishment of morphogen gradient during pattern formation (36–38). Those models use static cytonemes and weight functions pondering the quantity of received morphogen as the transport term of the equations. However, experimental evidence points that cytoneme dynamics can play an important role (22,23,28–30) and at present there are no data sustaining a pondered mechanism of signaling. In addition, the models assume a local source of morphogen, which is not true in most cases and there is also a theoretical study emphasizing the importance of using an extended source (39). Finally, previous models are not computationally implemented into a tool that can be used to test or load experimental data on cytoneme-mediated morphogen gradients.

In this work, we have developed a new dynamic model for cytoneme-mediated gradient formation, which validates this mechanism of cell signaling and has several advantages**:** 1) it was designed to be general enough to be applied to different morphogens or tissues, 2) it considers an extended morphogen source within a developing tissue, 3) the signaling is not based on weighted mechanisms, 4) it considers the dynamics of the

cytonemes and 5) it was implemented into a computational tool (Cytomorph), which makes it possible to develop *in silico* predictions for a variety of morphogens.

Results

Theoretical framework: Mathematical model

The gradient distribution can be generally determined as:

$$\frac{\partial u(\vec{x},t)}{\partial t} = P(u,\vec{x},t) + T(u,\vec{x},t) - D(u,\vec{x},t) \quad \text{(Eq-1)}$$

Where u is the concentration of a specific morphogen, $P(u,\vec{x},t)$ is the production term, $T(u,\vec{x},t)$ is the transport term and $D(u,\vec{x},t)$ is the degradation term.

To model the transport term for cytoneme-mediated morphogen signaling we focused in the main requirement of this type of signaling; the establishment of cell-to-cell membrane contacts for localized transmission. Thus, the core of our mathematical model is based on the determination of cytoneme contacts, in particular the contact distribution at receiving cells. Therefore, the transport term can be determined as:

$$T(u,\vec{x},t) = \alpha \cdot N(\vec{x},t) = \alpha \cdot \sum C(\vec{x},t) \quad \text{(Eq-2)}$$

Where $N(\vec{x},t)$is the total distribution of contacts and $C(\vec{x},t)$ is the contact function that englobes the contact mechanism for cytoneme signaling.

Experimentally, three types of cell-to-cell contacts have been reported for cytoneme intercellular communication (Reviewed in (40,41)) (Figure.1A-C):

Type 1: Cytonemes from receiving cells that contact signal-producing cell bodies (Fig.1A).

Type 2: Cytonemes from signal-producing cells that contact receiving cell bodies (Fig.1B).

Type 3: Cytonemes from both signal-producing and receiving cells that establish contact (Fig.1C).

To create a general model for cytoneme signaling, we considered the three experimentally described contact types to define the contact functions $C(\vec{x},t)$. Developmental tissues are usually compartmentalized into two cell populations that divide the morphogenetic field in producing and receiving regions. Therefore, we used this specific 1D geometry as a frame of reference (Fig.1D) to define the 1D contact functions $C(x,t)$. For simplicity, we used the discrete cell position $x=\phi$ as spatial coordinate.

The contact function type $C_x(\phi^{r,p})$ determines the possibility of contact between a receiving (ϕ^r) and a producing cell (ϕ^p), and they can be established in terms of a spatial condition as follows:

Types 1 and 2: In order to establish contacts, the distance between cells must be smaller than, or equal to, the maximum length of the cytonemes.

Type 3: In order to establish contacts, the distance between a producing and its receiving cell must be smaller than, or equal to, the sum of the maximum lengths of the cytonemes extending from these cells.

Which mathematically can be described for each type as:

- Type 1: $C_{rc\rightarrow pc}(\phi^{r,p},t)=\begin{cases}0 & if\ \ \phi^p \geq \lambda_r(t)-\phi^r \\ \psi(p,\phi^r) & if\ \ \phi^p < \lambda_r(t)-\phi^r\end{cases}$ (Eq-3.1)

- Type 2: $C_{pc\rightarrow rc}(\phi^{r,p},t)=\begin{cases}0 & if\ \ \phi^p \geq \lambda_p(t)-\phi^r \\ \psi(p,\phi^r) & if\ \ \phi^p < \lambda_p(t)-\phi^r\end{cases}$ (Eq-3.2)

- Type 3:

$$C_{cyt\rightarrow cyt}(\phi^{r,p},t)=\begin{cases}0 & if\ \ \phi^p < \lambda_r(t)-\phi^r \\ \psi(p,\phi^r) & if\ \ \lambda_p(t)-\phi^t \leq \phi^p < \lambda_r(t)+\lambda_p(t)-\phi^r \\ 0 & if\ \ \phi^p \geq \lambda_r(t)+\lambda_p(t)-\phi^p\end{cases} \quad \text{(Eq-3.3)}$$

The above equations describe the possible number of contacts between a receiving (ϕ^r) and a producing cell (ϕ^p), depending on their spatial location (ϕ^r, ϕ^p), the temporal dynamics of cytoneme length $\lambda_r(t)$ [$\lambda_p(t)$] and the probability of contact $\psi(p, \phi)$.

$\lambda_r(t)$ and $\lambda_p(t)$ describe the dynamics of elongation and retraction of cytonemes emanating from either receiving ϕ^ror producing ϕ^p cells. However, the linear growth usually assumed for the explicit definition of $\lambda_r(t)$ [$\lambda_p(t)$] does not match the dynamics observed in experimental data (30), where cytonemes not only can elongate and retract (Triangular behavior, Fig.1E), but also have intermediate stationary phases, during which the cytonemes maintain their maximum elongation (Trapezoidal behavior, Fig.1F). Therefore, in our model we considered the experimental results and the mathematically defined $\lambda_r(t)$ [$\lambda_p(t)$] using Triangular and Trapezoidal dynamics (see Supplementary Materials).

The probability of contacts $\psi(p, \phi)$ determines if there are contacts between cytonemes satisfying the minimum distance condition in a specific place ϕ with a probability of *p*. The function $\psi(p, \phi)$ takes the value of 1 in case of establishing a contact (see Supplementary Materials). This function $\psi(p, \phi)$, though, is only a probabilistic approximation to the real mechanism of signal transfer, since the cellular mechanisms to create a contact are starting to be elucidated (42) but not yet fully understood.

Computational framework: Model implementation

The general design of our model allows its application to most cytoneme-mediated morphogen gradients. Thus, to take full advantage of this approach, we created a Matlab-language-based software called Cytomorph, in which it is possible to simulate different experimental data and test different hypotheses *in silico*.

Cytomorph was designed with inputs divided into two sets (Fig.2A). The first set is loaded to Cytomorph via a spreadsheet (Fig.2A-1) encompassing all experimental distributions of cytoneme lengths and temporal distributions of elongation, retraction and stationary phases during cytoneme dynamics (See supplementary table S.1). The second set is loaded via a graphical user interface (GUI) (Fig.2A-2, see also Supplementary figure S.1). This group comprises: 1) average experimental values (e.g. cell size in a tissue and velocities of elongation and retraction), 2) parameters difficult to measure with the current experimental techniques (e.g. the contact probability and the temporal contact dynamics) and 3) features or parameters without experimental data but which are required for morphogen simulations (e.g. the number of cells needed for gradient formation and the role of cytoneme dynamics). A detailed illustration of features and parameters of the second group are described in the Supplementary figure S.1.

For an intuitive use of Cytomorph we designed a GUI to run simulations (Fig.2A,B) and Cytomorph was subdivided in different scripts and modules of the next three types: 1) A group of scripts for the GUI. 2) Modules to numerically simulate the cytoneme dynamics and to compute contacts and their spatial distribution over time. 3) A module to plot the simulated contacts together with different gradient properties (see Supplementary Materials for details).

To study cytoneme features and assess their role in the Hh gradient formation, Cytomorph was implemented to analyze different characteristics:

- *Contact distribution*: The contacts per cell along simulations (Fig.2C-1); violin plots are shown (Fig.2C-2) to visualize the contact distribution along simulations.
- *Signal variability*: To study the predicted *in silico* variability we computed the distribution of coefficients of variation per case (Fig.2C-3).

- *Temporal evolution*: To observe the number of contacts in each receiving cell per time lapse (Fig.2C-4) and the total evolution of contact distribution and gradient shape over simulated signaling time (Fig.2C-5).
- *Gradient distribution*: Assuming that each contact transmits the same amount of morphogen ($\alpha = const$ in eq-2), the distribution of the morphogen $u(\vec{x}, t)$ can be estimated through the $N(\vec{x}, t)$ calculated in the model (Fig.3C-6).

A detailed description of how the outputs were computed and calculated is in Material and Methods and Supplementary Materials sections.

Experimental framework: Model validation

To validate Cytomorph we used the Hedgehog (Hh) gradient formation in two different tissues of *Drosophila:* the imaginal wing disc and the abdominal histoblast nest. The latter has been used to study cytoneme dynamics as it allows *in vivo* imaging. Both tissues have the same cell distribution, in which the producing region (Posterior (P) compartment) signals over a receiving region (Anterior (A) compartment).

We first characterized and quantified the biological magnitudes needed as inputs for Cytomorph simulations. For length characterization, we overexpressed Ihog, a trans-membrane protein and co-receptor of the Hh pathway present in all epithelial cells, since its overexpression stabilizes cytonemes without affecting their length (30). This effect on cytoneme dynamics makes Ihog overexpression a good tool for cytoneme visualization at the basal side of fixed tissues, such as the wing imaginal disc (Fig.3A). Abdominal histoblast nests keep the same geometry of cell and cytoneme distribution in A and P compartments (Fig.3B and movie 1) as well as the same apico/basal polarity (Fig.3C). For the wild type dynamics of cytonemes, we used markers that do not affect cytoneme dynamics (Life-actin-RFP and mCD8-GFP) that we simultaneously overexpressed using

the binary systems UAS-Gal4 and QUAS-QF, allowing the *in vivo* visualization of both receiving (from A cells) and producing (from P cells) cytonemes (Fig.3C and movie 2).

Looking at the quantified length of cytonemes in the wing disc we observed a statistically significant difference, receiving A cytonemes being shorter than producing P cytonemes (Fig.3D). In addition, comparing both receiving and producing wing disc cytonemes with those of the abdominal histoblast nests (30), we observed that the former are significantly longer than the latter (Fig.3D). We also quantified the cell size in both tissues and found a difference in cell size: 3.05±0.65 μm in wing discs and 4.37±0.89 μm in abdominal histoblast nests (see Materials and Methods for the measurement protocol and the statistical study of this average values).

To quantify the Hh experimental gradient (and its experimental signal variability) as a validation for the model-simulated gradient profile, we analyzed the signal intensity of the endogenous Hh using a GFP fluorescent reporter (*Hh:GFP BAC*) in the two selected *Drosophila* tissues. Then, to compare the Hh gradient responses between different samples (see Materials and Methods and Supplementary figure S.2 for details), we also used a genetic tool (*EnhancerPtcRed*) that allows simultaneous visualization of Hh and the transcriptional response of its receptor Patched (Ptc) (Fig.4A). After statistical analysis, we found that, despite the tissue similarities, the Hh gradients are not identical (Fig.4B), with the gradient decaying faster in abdominal histoblast nests than in the wing imaginal discs. It is important to mention that in our cytoneme model the shape of the gradient is a consequence of the contact distribution (Supplementary figure S.3) and this distribution is due to cytoneme dynamics and cytoneme distribution along the tissue, which are elements experimentally settled. In addition, we observed that the range of the Hh gradient in both tissues can be determined by the sum of the maximum cytoneme

lengths, emphasizing again the importance of cytonemes as mechanism for gradient formation.

The scaling of Hh gradients between different tissues provides an opportunity to study the adaptability of our cytoneme model. Studying the parameter space after loading the experimental data (length, temporal dynamics of cytonemes and cell size), the *in silico* simulations have shown that our model was capable of predicting the shape of Hh gradients in the two tissues analyzed (blue fitted curve in Fig.4 C and D). In this way, we demonstrate the ability of the model to adapt to different biological conditions and correctly forecast the signaling gradient. The parameter space has been selected as a reference case for further simulations (Supplementary table S.2). Further information can be extrapolated when analyzing the parameter space used to fit the gradient. For example, model simulation for the Hh gradient in the wing disc agrees with the cytoneme contact type 3, which fits with the experimental data observed. Thus, modeling emphasizes the importance of the direct cytoneme-cytoneme (cyt-cyt) interaction for the correct development of the wing disc Hh gradient, so far assumed but not corroborated. As for the gradient in the abdominal histoblast nests, a lower probability for cyt-cyt interaction fits better with the experimental gradient, indicating that, in contrast with the wing disc tissue, in abdominal histoblasts, cyt-cyt interaction is not as critical as cytoneme to cell body contact.

Since many theoretical models still assume free diffusion as the mechanism for morphogen transport (10), we next compared our cytoneme model predictions with those of the classical diffusion-degradation model (see Supplementary Materials), and then both with experimental gradient measurements. Interestingly, in the case of the wing disc, both model predictions fall statistically within the experimental variability (Fig.4E), with the cytoneme model slightly closer to the experimental mean. However, this is not the

case for the abdominal histoblast nest where the diffusion model does not adapt and is not able to predict the gradient as accurately as the cytoneme model does (Fig.4F black). Indeed, the diffusion model would require the assumption of a three times smaller diffusion constant to fit simulations with experimental data in abdominal histoblast nests (Fig.4F red).

In silico framework: Model predictions

The model can be used to study the effect of different parameters on gradient formation. As examples, we have selected two parameters of which we could obtain experimental data (cytoneme length/cell size ratio and number of producing cells) and another parameter lacking experimental data (number of cytonemes per cell) and used Cytomorph simulations to predict their effects and values.

- *The ratio between cytoneme length and cell size* is a default unit used in the software to intuitively visualize the extent of cytonemes. In silico simulations showed that this ratio seems to be responsible of controlling the shape and length of the morphogen gradient (Fig.5A). Although this ratio also affects signal variability, this is not statistically significant in most cases (Fig.5A'). Therefore, after simulation we can conclude that both, length of cytonemes and cytoneme length/cell size ratio are key to understand how cytoneme signaling defines the shape of the gradient (Fig.5A'').

- *The number of signaling source cells* has been previously suggested as crucial for realistic gradient formation (39) and, therefore, we analyzed the effect of this parameter. In our model, we have observed that, starting count from the A/P compartment border, the first 5-7 rows of producing cells are key in shaping the Hh gradient (Fig.5B), while the next producing cell rows (rows 8-10) refine the gradient shape lowering the variability. Finally, increasing the number of Hh producing cells to more than 10 cell

rows does not affect the Hh gradient. This can be observed in both the amount of morphogen and the signal variability (Fig.5B and B'). Therefore, the number of producing cell rows is indeed important in the scaling and determination of the gradient shape (Fig.5B''). In contrast, analysis of the effect of receiving cell rows showed no effect in the Hh distribution (see supplementary figure S.4).

- *The density of cytonemes* is the number of cytonemes per cell, which is key in the amount of morphogen distributed (Fig.5C) and significantly affects signal variability (Fig.5C'), but it is not determinant for the gradient shape (Fig.5C''). Counter-intuitively, experimental variability can be estimated *in silico* (error bars versus green shaded area in Fig.5A) for a low number of cytonemes per cell, in agreement with the low number of cytonemes observed in wild type conditions (Fig.3C). These results point out that the shape of the gradient is mainly determined by the cytoneme behavior and not by the number of cytonemes per cell.

Hypotheses based on cytoneme behaviors

Cytomorph is an adaptable tool devised to answer different questions and test hypotheses on cytoneme mediated signaling. Since most of our working hypotheses are related to contact dynamics, we will next focus on how the three different contact types (Fig.1A-C) might affect gradient features. Types 1 and 2 can be considered mathematically the same, while type 3 should have an additional contribution, as both presenting and receiving cells emit contacting cytonemes. Our model predicts a significant effect in the gradient when considering the type 3 cytoneme contacts compared with those of types 1 or 2, as we found that the amount of morphogen (Fig.6A) and the length of the signal (Fig.6A') were doubled. Type 3 seems then to be the most probable situation for Hh gradient formation (Fig.6A), although types 1 and 2 can still be functional forms for other signaling situations.

Further analysis of contact dynamics properties using Cytomorph has also allowed the study of the reception/contact effect, currently not well understood due to lack of experimental approaches; it was defined in the model by the contact probabilistic function $\psi(p, \phi)$. In particular, we implemented in different Cytomorph modules three working hypothesis of the contact function $\psi(p, \phi)$:

1. A contact dynamic in which the probability of contact only depends on the condition that cytonemes are close enough; then the probability to contact is $\psi = \psi(p)$.
2. A contact dynamic in which different contacts can be established along the overlapping cytoneme membranes. This multiple-contacts approach was designed by the special contact function $\psi = \Psi(p)$.
3. A contact dynamic in which, in addition to the previous distance condition, the cell position is important and can be treated as a variable $\psi = \psi(p, \phi)$.

Comparing the first two hypothesized contacts, the *in silico* simulations showed that the overlapping multiple contacts function can significantly change the number of contacts and subsequently the amount of morphogen transferred (Fig.6B), also resulting in significant changes over signal variability (Fig.6B') and gradient shape (Fig.6B''). Similarly, comparison between cases 1 and 3 showed statistically significant changes in the number of contacts (amount of transmitted morphogen) and signal variability when including cell position as a variable (Fig.6 C and C'). In addition, after the analysis of different scaling across receiving cells we could also infer that gradient distribution was affected (Fig.6C''), with case 3 showing a faster and more linear decay as a consequence of its dependence on cell position (see Supplementary Materials).

Since our results suggest that the contact probability function only depends on the variable *p*, we carried on an *in silico* study to test the impact of this variable over gradient

features. Interestingly, model simulations for different values of *p* only significantly contribute to the amount of morphogen transferred (Fig.6D), but they do not disturb neither the variability nor the shape of the morphogen gradient (Fig.6D' and D'').

Cytoneme dynamics in Hh gradient evolution

To this point we have validated Cytomorph in steady state conditions (Fig.5 C and D), and from now on we will test its capability to study temporal aspects during gradient formation. For this purpose, we performed fluorescence recovery after photobleaching (FRAP) experiments in the abdominal histoblast nest. In this tissue, the gradient is established previous to histoblast migration and it allows the dynamic characterization of the Hh signaling gradient by *in vivo* recording (movie 3).

Previous to photobleaching a reference Z-stack was taken and the signal was bleached to 80-90% of the initial maximum value (Fig.7A); recovery was then recorded in a Z-stack every 45 seconds. To automatize the acquisition of the gradient profile, a FIJI macro was written. The results showed that the Hh gradient recovered up to 92% of the initial value in less than 50 minutes (Fig7.B), while the receptor graded response (*EnhancerPtcRed*) presented a 64% recovery in the same time. (Fig7.C). This difference in the percentage of recovery was expected, as there is a delay in the reporter response, which requires both transcription and translation. To validate the temporal evolution of the model, we then simulated the Hh gradient in histoblast nests using Cytomorph (Fig.7D) and compared the predicted and the experimental curves. As we can observe in Fig.7E, the temporal prediction and the experimental signal recovery are the same, corroborating the capacity of Cytomorph to predict the temporal evolution of the gradient.

Cytomorph could also be used to solve pending questions regarding cytoneme dynamics. In particular, we were intrigued by the two detected dynamic behaviors of

cytonemes, Triangular and Trapezoidal (30). To address if these two cytoneme behaviors represent any advantage, we altered the fraction of the cytoneme population with each behavior and simulated how this changes could affect the gradient distribution and its variability (Fig.7 F and F'). It was especially interesting to find out that Triangular cytonemes have a stronger impact in the tail of the gradient, while Trapezoidal cytonemes have greater impact near the morphogen source (Fig.7F'').

The experimental data show the importance of the cytoneme dynamics for gradient formation (22,23,28–30). Our simulations also showed that dynamic and static cytonemes generate different gradient shapes (supplementary figure S.5). This is noteworthy since many theoretical models do not consider this temporal aspect and our results indicate that using dynamic cytonemes the predicted gradient better fits the experimental data (supplementary figure S.5). It should be remembered that the temporal dynamics of the contacts is not yet well defined and it is experimentally difficult to unravel how dynamic contacts coordinate with growth during gradient formation. Cytomorph can be used to study plausible biological scenarios for Hh signaling, even in the absence of data. In fact, simulations of contacts and growth (supplementary figure S.5) allows to study the dynamic of signaling and reflect the complexity in the coordination of different cytoneme features in the formation of a gradient.

Robustness of cytoneme signaling

Failures can occur during the development of organisms, but cell signaling has been shown to have a robust control mechanism (43–45) in which a combination of parameters can compensate for a possible developmental failure. In this context, Cytomorph can also serve to identify interactions or compensation mechanisms; as an example, we have found an interesting interaction between the number of producing cells and the density of cytonemes per cell: a reduction in the number of producing cells can be compensated by

an increase in the number of cytonemes per cell (supplementary figure S.6). Both predicted gradients fall within the experimental variability, creating a "functional" gradient that should be able to activate the same target genes.

Discussion

In this work, we present a general *in silico* model for morphogen gradient formation considering that the morphogen dispersion is mediated by cytonemes. In particular, we demonstrate that this model validates a mechanism of cytoneme-mediated Hh gradient that can be extrapolated to other morphogens. We have implemented our model in an open computational software (Cytomorph), which allows the introduction of experimental data to study the role of different biological parameters. With this approach we try to overcome the previous lack of connection between theoretical models and experimental data in cytoneme mediated cell signaling. To improve our understanding of how specific cytoneme features impact the gradient properties, Cytomorph is able to plot results in graphs showing the final shape of the morphogen distribution, the number of contacts, the signal variability, the time course and the gradient scaling. To facilitate the use of this tool, we also designed a GUI allowing straightforward control of the software commands.

Model validation

To experimentally validate the model and its adaptability to real gradient predictions, we studied the Hh gradient formation in two different *Drosophila* tissues: wing imaginal discs and abdominal histoblast nests. Using different genetic tools, we experimentally quantified several parameters in both tissues, such as the length of cytonemes, the cell size and the Hh gradient distribution. Cytomorph was able to predict the Hh scaling and correctly simulate the signal gradients in both tissues, emphasizing the involvement of

cytonemes for a correct signaling. Although the quantified gradient scaling in these two tissues had not been previously characterized, we expected them to be different because, despite their similarities, both systems have different behaviors: while the wing disc is an expanding but static epithelium, the abdominal histoblasts divide and migrate simultaneously reducing, for instance, the probability of cyt-cyt contacts, as our model suggests.

Cytoneme model versus diffusion model

The diffusion model is still the mathematical model most commonly used in biophysics, although the biochemical properties of most morphogens argue against their transport via Brownian motion. Comparing our cytoneme model with the classic diffusion-degradation model, we found that our model thoroughly predicts the shape of the Hh gradient in two different tissues, the wing imaginal discs and the abdominal histoblast nests. The diffusion model, however, required a readjustment of the diffusion constant to predict the Hh gradient in the abdominal histoblast nests. It is not clear why the diffusion constant has to be different for the same protein in similar epithelial tissues. Nevertheless, it is important to point out that the measurement of the diffusion constant is an effective parameter that summarizes a collective behavior and does not give information regarding the transport mechanism involve. Actually, it has been described that the diffusion coefficients can significantly vary depending on the morphogen, the tissue and the experimental approach (46).

***In silico* study of cytoneme features**

After the experimental validation of Cytomorph, we studied *in silico* different aspects of cytoneme-mediated signaling as a way to understand the role of cytoneme features and to be able to generate hypotheses regarding this signaling mechanism. We initially tested

the cytoneme length/cell size ratio, a parameter for which we already had experimental data, and our simulations suggested that it is a crucial parameter for the Hh gradient scaling but not for the variability of the signal. This model prediction was experimentally supported in abdominal histoblast nests and in imaginal wing discs.

Theoretical analysis (39) emphasizes the importance of considering an extended source to predict realistic gradients, however previous models do not take this element into account. Therefore, we used Cytomorph to clarify the effect of an extended source in shaping the gradient. The resulting simulations gave a detailed description of how the gradient is affected by changing the number of cell rows involved in the production of morphogen in a tissue.

Cytomorph also provides the possibility to analyze the effect on gradients of parameters for which there are no experimental data, such as the number of cytonemes per cell. Interestingly, our results suggest that this particular parameter is key for both the variability of the signal and the amount of transmitted morphogen but not for the distribution or the scaling of the gradient. Moreover, simulations also allowed to estimate the probable number of cytonemes per cell.

In parallel with cytonemes parameters we have also studied other features of the cytoneme-mediated signaling. By observing the effect of different types of signaling contacts, our model predicts that the type 3 will be different from types 1 and 2, since the amount of transmitted morphogen and the length of the gradient increase due to cyt-cyt contacts. In agreement with experimental observations, our *in silico* results have shown that type 3 cytoneme interaction is the most likely situation for Hh gradient formation in the wing imaginal disc.

Previous approaches to cytoneme signaling used weight functions, with a dependence on cell position, to ponder the quantity of received morphogen. To ascertain

if this dependence is required, we tested three different hypotheses for the contact function $\psi(p, \phi)$. From the resulting predictions we could conclude that the simplest case $\psi = \psi(p)$ fits the gradient distribution better than $\psi = \psi(p, \phi)$ with linear decay. In contrast with previous approaches, our model suggests that this contact probability not requires of a pondered mechanism based on cell position. Instead, what determines the exponential shape of the gradient is the distribution of contacts along receiving cells. Finally, we studied the effect of the probability of contact p in the gradient properties. Our results showed that this parameter has a significant impact over the amount of morphogen transmitted but not over the signal variability or the gradient shape.

Cytoneme dynamics in Hh gradient formation

One of the main advantages of our model was the inclusion of the temporal dynamics in the equations, which has been experimentally found to play a significant role in the correct activation of the target genes during development. To validate the temporal dynamics of our model we performed experiments to study the temporal recovery of the Hh signal after photobleaching (FRAP technique), and then compared this data with our model simulations. Comparison of the predicted and the experimental gradient curves proved that our dynamic model is able to simulate physiological temporal features.

We then used Cytomorph to study the role of the two types of cytoneme behavior (Triangular and Trapezoidal) observed experimentally. Our simulations allowed us to generate the hypothesis that different ratios of Triangular to Trapezoidal dynamics might have a distinctive impact on specific regions of the Hh gradient, suggesting the importance of these cytoneme behaviors on the precise spatial control of the gradient shape. Besides the generation of this new hypothesis, our simulations also show that the

proportion 50% Triangular and 50% Trapezoidal dynamics would fits better the experimental data, and this happens to be the proportion found experimentally (30).

Our simulations point out that static and dynamic cytonemes give rise to quite different Hh gradient. Consequently, this characteristic of cytoneme signaling should be included in theoretical models to study cytoneme signaling. Moreover, cytoneme temporal dynamics could provide robustness to the progressive establishment of signaling gradients, an advantage for both growing (wing imaginal discs) and migrating while growing systems (abdominal histoblast nests). Static cytonemes are less likely to adapt to tissue changes, increasing the probability of failure, while dynamic cytonemes can allow constant regulation of the gradient shape throughout development. Nevertheless, other static tubular structures, such as tubulin-based channels, could be significant for other morphogens or biological models (47).

The *in silico* model also emphasizes the role of different features in the gradient properties and, more importantly, predicts that the shape of the gradient is a consequence of the contact distribution; in turn, this distribution is due to cytoneme dynamics and cytoneme distribution along the tissue. In fact, the model suggests that during the correct establishment of graded distribution, cytoneme dynamics are more critical than the amount of available morphogen from producing cells. This hypothesis has been recently corroborated experimentally for several morphogens. The analysis of the dispersion of Hh, Wg, and Dpp in the Drosophila wing imaginal disc indicates that their delivery to target cells is regulated since an increment in their gene doses does not alter the extent or shape of their gradients (48). For Hh signaling, the receiving cells take up less than the 5% of Hh produced and under conditions of Hh production up to 200% of the normal amount, neither the protein uptake nor the extent of the gradient changes. These findings

show that the amount and destination of delivered morphogens are regulated, all in agreement with a cytoneme model but not with a diffusion model.

Finally, although our interest along this work has been focused on identifying individual roles for different cytoneme parameters that could affect the morphogen gradient formation, Cytomorph was also able to detect interactions or compensation mechanisms between cytoneme features. This kind of interactions, able to compensate malfunctions, emphasizes the robustness of the cytoneme model as a signaling mechanism. In addition, based on uncomplicated mathematical premises, our model improves the understanding of cytoneme signaling mechanism and can be adapted to different biological systems. This adaptability is due to the modular architecture used to design the Cytomorph software, in which new modules can be added to test emerging biological hypotheses, as soon as new findings or experimental conditions become available.

Material and Methods

Experimental methods

Drosophila lines

Drosophila melanogaster stocks were maintained according to protocols described in Ashburner manual (49). Crosses were maintained at 18^0C until the time of gene expression induction The description of mutations, insertions and transgenes is available at Fly Base (http://flybase.org).

The following drivers were used to induce ectopic expression using the Gal4/UAS (50) and QUAS-QF (51) systems: tubGal80^{ts} (Bloomington *Drosophila* Stock Center, BDSC),

hh.Gal4 (52), *ptc.Gal4* (53) and *Hh-QF* (generated by Ernesto Sánchez-Herrero, CBMSO).

Overexpression stocks: The *pUAS*-transgene strains used were: *UAS.ihog-YFP* (54) *and UAS.LifeActinRFP (*BDSC *58362).* The QUAS-transgene strains used were: *QUAS.mCD8-GFP* (BDSC 30002).

Other stocks: *EnhancerPtcRed* (Kyoto stock center, DGRC 109138) *and Hh:GFP BAC* (55).

Experimental data acquisition and quantification in wing imaginal discs

Laser scanning confocal microscopes (LSM700 and LSM800 Zeiss) were used for confocal fluorescence imaging of imaginal discs. Fluorescence signal of *Hh:GFP BAC* protein and *EnhancerPtcRed* reporter were obtained using 40 x magnification and taking Z-stacks with a step size of 0.7-1 μm. Fiji software (ImageJ software, National Institutes of Health) was used for image processing and analysis.

- *Filopodia extension*

Cytonemes were labeled overexpressing UAS-Ihog-YFP in either Hh-Gal4 (P compartment) or Ptc-Gal4 (A compartment) domains for 24-48h before dissection. The length extension of cytonemes was manually measured using the Straight tool from FIJI software. The statistical analysis and software simulations were done using a total of 984 cytonemes, 729 in the P compartment and 255 in the A compartment.

- *Cell diameters for gradient normalization*

Since the software computes the data in cell diameters, to compare the experimental data with model simulations, it is important to know the characteristic cell diameter in μm of each specific tissue studied. For the normalization of the gradient length, we manually measured approximately 100 cells along the X-axis in each wing imaginal disc (n=19).

- *Hh gradient imaging in wing discs.*

Hh protein gradient and the graded response of *ptc* enhancer reporter were measured experimentally using Plot profile tool of FIJI taken an average Z-stack projection to get all the morphogen distribution along apicobasal sections of the wing disc epithelium. The fluorescence profiles of the corresponding channel for the *Hh:GFP BAC* and *EnhancerPtcRed* signals were measured in a 90x35 μm^2 region of the A compartment with the start positioned at ≈25 μm from the A/P border inside the P compartment.

- *Mathematical protocol for the Hh gradient data.*

The Hh protein gradient and *ptc* enhancer reporter gradient response in wing discs and their experimental variabilities were estimated using 19 different wing disc samples, as follows: the background was estimated measuring the mean signal level over a 20 μm region in areas in which each reporter genetic tool is not active; for the *ptc* reporter signal, the region corresponds to the entire P compartment, while for Hh protein the region corresponds to the A compartment cells located away from the A/P compartment border. After subtracting the background, the intensity was normalized with the mean of the maximum intensities (3 values for the region of maximum *ptc* enhancer reporter expression and the whole P compartment signal for Hh protein levels). Finally, to compare the resulting data, we translated the measured profiles to the same reference origin; for the beginning of the Hh gradient we used the A/P compartment border. This origin was mathematically estimated using the well-defined sharp increase in *ptc* expression at the A/P compartment border. The graphic steps of the process are depicted in the supplementary figure S.2.

Data acquisition and quantification for *in vivo* imaging in abdominal histoblast nests

Pupal abdominal histoblasts imaging was performed in a chamber to seat and orient the pupae to look under the microscopy as described in (29). The dorsal abdominal segment A2 was filmed using 40x magnification; Z-stacks of around 30 μm of thickness with a step size of 1.1-1.3 μm were taken using a LSM800 confocal microscope. The overnight movies of the Hh-GFP gradient and the *ptc-RFP* enhancer graded response during the histoblast migration (movie 3) were done recording Z-stacks every 2 min. For optimal recording of dynamic cytonemes, *in vivo* experiments using at the same time Gal4 and Q systems were taken in different conditions (Z-tack of 18.5 μm with a step size of 0.5 μm every-one minute). Also movie 2 (see some sequences in Fig.3) was computationally treated using a deconvolution method (Huygens software) for cleaning the fluorescence signal.

- *Cell diameters for gradient normalization.*

The cell diameters for Hh and *ptc* profile normalizations were measured for 14-32 different histoblasts per pupae along the X-axis (n=9). Since we did not find statistical differences in cell diameters between A ($\phi^{anterior}$ = 4.285 ± 0.886 μm with n=228) and P compartment cells ($\phi^{posterior}$ = 4.453 ± 0.887 μm with n=245). We used the average value (ϕ = 4.37 ± 0.89 μm, n=473) for abdominal histoblast simulations.

- *Imaging Hh gradient in abdominal histoblast nests.*

The Hh protein gradient and *ptc* enhancer reporter signals were measured using the Plot profile tool of FIJI in an average Z-stack projection, as we have done for the wing imaginal disc samples. In each channel, profiles were measured for the same region of 200x130 pixels (51.51x33.48 μm^2) located in the A compartment close to the A/P compartment border.

- *Mathematical protocol for Hh Gradient data.*

The experimental variability of Hh signal and its gradient in abdominal histoblast nests were estimated using 14 different regions (in the A compartment close to de A/P border) extracted from 9 pupae. In each sample, the background signal was subtracted using the corresponding minimum value and then the intensity was normalized with the maximum value in each case. Finally, the profiles were translated to the same position using the maximum as a reference.

- *Statistical analysis of filopodia extensions*

To study the parametric behavior of the data, we first performed a Shapiro-Wilk normality test. After testing the non-parametric condition of the experimental distributions, we studied the significance using the Wilcoxon rank Sum test of homogeneity of variances (Implemented in Matlab2015a).

- *Data analysis of cytoneme dynamics*

The experimental data of filopodia dynamics have been taken from previous studies (30). Here, we have statistically studied in R language the differences between the times of the elongation, retraction and stationary phases of Triangular and Trapezoidal behaviors using a Kolmogorov-Smirnov statistical analysis (Supplementary table S.3), as we observed statistically significant differences between Triangular and trapezoidal times we develop the model to consider both behaviors.

Analysis of the Hh gradient formation by FRAP experiments

Fluorescence recovery after photobleaching (FRAP) is a method to study temporal evolution of fluorescent signals. An initial z-tack covering from apical to basal sections of the tissue was performed using Zeiss-LSM800 confocal microscopy to record the pre-breaching conditions of the sample. To avoid damaging the tissue, the photobleaching

was done over a ROI of (48.7x61.3 μm^2) in a region located at the A/P compartment border (we used *ptc* expression as a reference for the A/P compartment border (Fig7.A)). Photobleaching of the abdominal histoblast nests was done by series of short expositions of 488 nm laser at 100% intensity until the signal at that z-plane reached less than 10% of the initial value. Since the Hh signal is present through apicobasal length of the tissue, we repeated the photobleaching conditions 7-10 times at different sections covering the total apico-basal tissue length. To obtain the Hh signal recovery over time we recorded the same region used in the pre-bleach z-stack conditions every 45 seconds immediately after photobleaching.

The acquired image samples of the photo-bleached ROI area were then treated with the imaging protocol described above (quantification of the wild type Hh gradient in abdominal histoblast nets). Since the resulting file is not a simple image but a temporal sequence of images, we automatized the process creating a macro script in Fiji that measures the Hh and Ptc profiles over time in the region where the photobleaching was performed. Since the experimental conditions can generate undesired photobleaching, a control of the Hh signal intensity in the P compartment was also measured each time. To study the FRAP recovery we used the previously described mathematical protocol that translates all signals to the same origin, but normalization was done using the P compartment control values as follow:

$$\frac{Intensity\ where\ FRAP\ was\ done - background\ signal}{control\ intensity - background\ signal}$$

This equation is used in FRAP experiments to mathematically remove the possible undesired photobleaching in the recovery measurements.

Finally, to visualize the recovery evolution of the pre-bleaching gradient in percentages, the resulting values were normalized to the pre-bleaching maximum value.

All the samples studied (n=6) showed the same recovery tendency for Hh and *ptc* expression profiles than the representative case shown in Figure 7 B and C.

Theoretical and computational methods

Software code:

Cytomorph was generated implementing the cytoneme model in Matlab language (MatlabR2015a). Since Cytoneme-mediated signaling has been reported for many different morphogens and for different animal systems, our goal was that Cytomorph could be used as a computational tool to help other scientist. We then decided to develop Cytomorph as an open source software under a 3-clause BSD FOSS license. The software code and a manual for users are available in the software repository:

https://github.com/AdrianA-T/cytomorph

The available version of Cytomorph has been divided into different modules that can be updated to incorporate new discoveries in the formation of gradients, these modules can also be remodeled to simulate specific requirements of the system under study.

Units used in the model:

The frame of reference selected for the model is summarized in Fig.1D. The distance expressed in terms of cell diameters was selected for two main reasons: first, it is an intuitive unit commonly used in biology, that helps to visualize the data; and second, for practical reasons, since the mathematical equation of the model and the software code implementation are simplified using this distance unit. Therefore, the distance estimated through the experimental data (initially in μm) was normalized to cell diameters dividing by the average cell size, as described in cell size measurement protocols. The temporal unit used in this model was the second, so, the time calculated in the model from the *in*

vivo dynamic cytonemes were expressed in seconds. The rest of variables in the model are either dimensionless or expressed in terms of cell diameters and seconds.

Requirements to compare experimental data of the gradient with the theoretical contact function.

The conditions to compare *in silico* simulations with experimental data have been estimated in the supplemental material and can be summarized as:

- Mathematically: The degradation rate of the morphogen should be taken into account.
- Experimentally: Confocal images must have been taken according to the linear gamma function and within the limits of the acquisition range.

***In silico* simulations**

- *Numerical simulations:*

Each *in silico* prediction was computed 2000 times per simulation and case, the different values obtained over those 2000 times were used to generate the predicted gradient for those conditions. The standard deviation of the data obtained of those 2000 times was used as the expected signal variability.

- *Parameters and data for simulations:*

Supplementary table S.2 details the parameters used in each simulation. The updated experimental data in those simulations were obtained from the already described measurements of the wing disc cytoneme length or the average cell diameter (ϕ= 4.37 ± 0.89 μm for abdominal histoblasts and ϕ= 3.05 ± 0.65 μm for wing disc cells). The experimental cytoneme dynamics were obtained from previous studies (30). Finally, the

average Hh gradient profiles obtained in the validated simulations was used in both systems. The degradation rate of Hh was obtained from a previous study (56).

- *Statistical analysis.*

The Wilcoxon rank sum test was performed per pairs and the resulting p-values were graphically coded in matrixes with a green color that is graded depending on the significance. The code used was: black for no significance (= n.s) and dark green to light green respectively for the p-values: * = p-value < 0.05, ** = p-value < 0.01, *** = p-value < 0.001, **** = p-value < 0.0001.

As mentioned, *in silico* predictions were computed over 2000 times per simulation in each case; the different values obtained over those 2000 samples were used for the statistical analysis using Wilcoxon rank sum test (Implemented in Matlab2015a).

For the Coefficient of variation, we divided the 2000 simulations in 100 subgroups of 200 samples each. Then the coefficient of variation distribution per case was performed over those 100 subgroups. Finally, we used those 100 values per case for the posterior statistical analysis of the signal variability using the coefficient of variation.

- *Simulations of the diffusion-degradation model*

Simulations for the diffusion-degradation model (next equation) were performed using in Matlab2015a language using *pdepe* function for 1-D parabolic and elliptic PDEs.

$$\begin{cases} PDE: & \dfrac{\partial u}{\partial t} = D\Delta u - \delta \cdot u & \\ BC: & u(0,t) = \langle u_{exp}^{N} \rangle_{x=0} & 0 < t < \infty \\ & \dfrac{\partial u(L,t)}{\partial t} = 0 & 0 < t < \infty \\ IC: & u(x,0) = 0 & 0 < x \leq L \end{cases}$$

The boundary and initial conditions are required to solve the equation. We decided to use the condition of the morphogen flux equal to zero at the tissue end (L) $\frac{\partial u(L,t)}{\partial t} = 0$. This derivate boundary condition is commonly used and in biological terms means that the morphogen cannot escape from the tissue. The initial conditions the morphogen gradient is zero $u(x, 0) = 0$ since there is no previous diffusion of the morphogen. Finally, to have more precise experimental conditions for the diffusion simulations, the boundary condition at the origin has been selected as the experimental average of the maximum values for the normalized Hh gradient $u(0, t) = \langle u^N_{exp} \rangle_{x=0}$.

The same experimental data were used for both: cytoneme and diffusion models. A table detailing the parameters can be found in supplementary material (Supplementary table S.4).

References and Notes

1. Varjosalo M, Taipale J. Hedgehog: Functions and mechanisms. Vol. 22, Genes and Development. Genes Dev; 2008. p. 2454–72.
2. Lawrence PA. Morphogens: How big is the big picture? Vol. 3, Nature Cell Biology. Nat Cell Biol; 2001.
3. Akiyama T, Gibson MC. Morphogen transport: Theoretical and experimental controversies. Vol. 4, Wiley Interdisciplinary Reviews: Developmental Biology. John Wiley and Sons Inc.; 2015. p. 99–112.
4. Turing AM. The chemical basis of morphogenesis. Philos Trans R Soc Lond B Biol Sci. 1952 Aug 14;237(641):37–72.
5. Wolpert L. Positional information and the spatial pattern of cellular differentiation. J Theor Biol. 1969 Oct 1;25(1):1–47.

6. Bozorgui B, Teimouri H, Kolomeisky AB. Theoretical analysis of degradation mechanisms in the formation of morphogen gradients . Cit J Chem Phys. 2015;143:25102.

7. Teimouri H, Kolomeisky AB. The role of source delocalization in the development of morphogen gradients. Phys Biol. 2015;12:26006.

8. Teimouri H, Kolomeisky AB. Development of morphogen gradient: The role of dimension and discreteness. Cit J Chem Phys. 2014;140:85102.

9. Iber D, Tanaka S, Fried P, Germann P, Menshykau D. Simulating tissue morphogenesis and signaling. Methods Mol Biol. 2015;1189:323–38.

10. Kondo S, Miura T. Reaction-diffusion model as a framework for understanding biological pattern formation. Vol. 329, Science. American Association for the Advancement of Science; 2010. p. 1616–20.

11. Gradilla AC, Guerrero I. Cytoneme-mediated cell-to-cell signaling during development. Vol. 352, Cell and Tissue Research. Cell Tissue Res; 2013. p. 59–66.

12. Ramírez-Weber F a., Kornberg TB. Cytonemes: Cellular processes that project to the principal signaling center in Drosophila imaginal discs. Cell. 1999;97(5):599–607.

13. Gradilla AC, Guerrero I. Cytoneme-mediated cell-to-cell signaling during development. Cell Tissue Res. 2013;352(1):59–66.

14. Kornberg TB. Cytonemes and the dispersion of morphogens. Vol. 3, Wiley Interdisciplinary Reviews: Developmental Biology. John Wiley and Sons Inc.; 2014. p. 445–63.

15. González-Méndez L, Gradilla AC, Guerrero I. The cytoneme connection: Direct long-distance signal transfer during development. Dev. 2019 May 1;146(9).

16. Hsiung F, Ramirez-Weber FA, David Iwaki D, Kornberg TB. Dependence of Drosophila wing imaginal disc cytonemes on Decapentaplegic. Nature. 2005 Sep 22;437(7058):560–3.

17. Roy S, Huang H, Liu S, Kornberg TB. Cytoneme-mediated contact-dependent transport of the Drosophila decapentaplegic signaling protein. Science. 2014;343(6173):1244624.

18. Huang H, Kornberg TB. Myoblast cytonemes mediate Wg signaling from the wing imaginal disc and Delta-Notch signaling to the air sac primordium. Elife. 2015 May 7;4(MAY).

19. Stanganello E, Hagemann AIH, Mattes B, Sinner C, Meyen D, Weber S, et al. Filopodia-based Wnt transport during vertebrate tissue patterning. Nat Commun. 2015;6:5846.

20. Roy S, Hsiung F, Kornberg TB. Specificity of Drosophila cytonemes for distinct signaling pathways. Science. 2011;332(6027):354–8.

21. Rojas-Ríos P, Guerrero I, González-Reyes A. Cytoneme-mediated delivery of Hedgehog regulates the expression of bone morphogenetic proteins to maintain germline stem cells in Drosophila. PLoS Biol. 2012 Apr;10(4).

22. Bischoff M, Gradilla A-C, Seijo I, Andrés G, Rodríguez-Navas C, González-Méndez L, et al. Cytonemes are required for the establishment of a normal Hedgehog morphogen gradient in Drosophila epithelia. Nat Cell Biol. 2013;15(11):1269–81.

23. Sanders TA, Llagostera E, Barna M. Specialized filopodia direct long-range transport of SHH during vertebrate tissue patterning. Nature. 2013 May 30;497(7451):628–32.

24. De Joussineau C, Soulé J, Martin M, Anguille C, Montcourrier P, Alexandre D.

Delta-promoted filopodia mediate long-range lateral inhibition in Drosophila. Nature. 2003 Dec 4;426(6966):555–9.

25. Cohen M, Georgiou M, Stevenson NL, Miodownik M, Baum B. Dynamic Filopodia Transmit Intermittent Delta-Notch Signaling to Drive Pattern Refinement during Lateral Inhibition. Dev Cell. 2010;19(1):78–89.

26. Hamada H, Watanabe M, Lau HE, Nishida T, Hasegawa T, Parichy DM, et al. Involvement of Delta/Notch signaling in zebrafish adult pigment stripe patterning. Dev. 2014 Jan 15;141(2):318–24.

27. Eom DS, Bain EJ, Patterson LB, Grout ME, Parichy DM. Long-distance communication by specialized cellular projections during pigment pattern development and evolution. Elife. 2015 Dec 23;4(DECEMBER2015).

28. Nahmad M, Stathopoulos A. Dynamic interpretation of hedgehog signaling in the Drosophila wing disc. PLoS Biol. 2009;7(9).

29. Seijo-Barandiarán I, Guerrero I, Bischoff M. In vivo imaging of hedgehog transport in drosophila epithelia. In: Methods in Molecular Biology. Humana Press Inc.; 2015. p. 9–18.

30. González-Méndez L, Seijo-Barandiarán I, Guerrero I. Cytoneme-mediated cell-cell contacts for hedgehog reception. Elife. 2017 Aug 21;6.

31. Simon E, Aguirre-Tamaral A, Aguilar G, Guerrero I. Perspectives on Intra- and Intercellular Trafficking of Hedgehog for Tissue Patterning. J Dev Biol. 2016;4(4):34.

32. Bressloff PC, Kim H. Bidirectional transport model of morphogen gradient formation via cytonemes. Phys Biol. 2018;15(2).

33. Kim H, Bressloff PC. Impulsive signaling model of cytoneme-based morphogen gradient formation. Phys Biol. 2019 Jul 22;16(5):056005.

34. Kim H, Bressloff PC. Direct vs. synaptic coupling in a mathematical model of cytoneme-based morphogen gradient formation. SIAM J Appl Math. 2018 Sep 4;78(5):2323–47.

35. Bressloff PC, Kim H. Search-and-capture model of cytoneme-mediated morphogen gradient formation. Phys Rev E. 2019 May 1;99(5).

36. Teimouri H, Kolomeisky AB. New Model for Understanding Mechanisms of Biological Signaling: Direct Transport via Cytonemes. J Phys Chem Lett. 2016 Jan 7;7(1):180–5.

37. Vasilopoulos G, Painter KJ. Pattern formation in discrete cell tissues under long range filopodia-based direct cell to cell contact. Math Biosci. 2016 Mar 1;273:1–15.

38. Kondo S. An updated kernel-based Turing model for studying the mechanisms of biological pattern formation. J Theor Biol. 2017;414(November 2016):120–7.

39. Dalessi S, Neves A, Bergmann S. Modeling morphogen gradient formation from arbitrary realistically shaped sources. J Theor Biol. 2012 Feb 7;294:130–8.

40. Sagar, Pröls F, Wiegreffe C, Scaal M. Communication between distant epithelial cells by filopodia-like protrusions during embryonic development. Dev. 2015 Feb 15;142(4):665–71.

41. Pröls F, Sagar, Scaal M. Signaling filopodia in vertebrate embryonic development. Vol. 73, Cellular and Molecular Life Sciences. Birkhauser Verlag AG; 2016. p. 961–74.

42. Huang H, Liu S, Kornberg TB. Glutamate signaling at cytoneme synapses. Science (80-). 2019 Mar 1;363(6430):948–55.

43. Kang HW, Zheng L, Othmer HG. The effect of the signalling scheme on the robustness of pattern formation in development. Interface Focus. 2012 Aug

6;2(4):465–86.

44. Irons DJ, Wojcinski A, Glise B, Monk NAM. Robustness of positional specification by the Hedgehog morphogen gradient. Dev Biol. 2010;342(2):180–93.

45. Lei J, Wan FYM, Lander AD, Nie Q. Robustness of signaling gradient in Drosophila wing imaginal disc. Discret Contin Dyn Syst - Ser B. 2011 Oct;16(3):835–66.

46. Rogers KW, Schier AF. Morphogen gradients: From generation to interpretation. Annu Rev Cell Dev Biol. 2011;27:377–407.

47. Holzer T, Liffers K, Rahm K, Trageser B, Özbek S, Gradl D. Live imaging of active fluorophore labelled Wnt proteins. FEBS Lett. 2012 Jun 4;586(11):1638–44.

48. Hatori R, Kornberg TB. Regulated delivery controls Drosophila Hedgehog, Wingless and Decapentaplegic signaling. bioRxiv. 2020 Aug 13;2020.08.12.247759.

49. Ashburner M. Drosophila: A laboratory Handbook. Cold Spring Harbor Laboratory; 1989.

50. Brand AH, Perrimon N. Targeted gene expression as a means of altering cell fates and generating dominant phenotypes. Development. 1993/06/01. 1993;118(2):401–15.

51. Potter CJ, Tasic B, Russler E V., Liang L, Luo L. The Q system: A repressible binary system for transgene expression, lineage tracing, and mosaic analysis. Cell. 2010 Apr;141(3):536–48.

52. Tanimoto H, Itoh S, Ten Dijke P, Tabata T. Hedgehog creates a gradient of DPP activity in Drosophila wing imaginal discs. Mol Cell. 2000 Jan 1;5(1):59–71.

53. Hinz U, Giebel B, Campos-Ortega JA. The basic-helix-loop-helix domain of Drosophila lethal of scute protein is sufficient for proneural function and activates neurogenic genes. Cell. 1994 Jan 14;76(1):77–87.

54. Callejo A, Bilioni A, Mollica E, Gorfinkiel N, Andrés G, Ibáñez C, et al. Dispatched mediates Hedgehog basolateral release to form the long-range morphogenetic gradient in the Drosophila wing disk epithelium. Proc Natl Acad Sci U S A. 2011;108(31):12591–8.

55. Chen W, Huang H, Hatori R, Kornberg TB. Essential basal cytonemes take up hedgehog in the Drosophila wing imaginal disc. Dev. 2017 Sep 1;144(17):3134–44.

56. Fried P, Sánchez-Aragón M, Aguilar-Hidalgo D, Lehtinen B, Casares F, Iber D. A Model of the Spatio-temporal Dynamics of Drosophila Eye Disc Development. PLoS Comput Biol. 2016 Sep 1;12(9).

Acknowledgements

We are grateful to Pedro Ripoll, Ana-Citlali Gradilla, Nicole Gorfinkiel, David G. Míguez, and Juan Soler for their advice and comments on the manuscript. Thanks to Dagmar Iber for hosting A.A-T and her advice. We also thanks to Confocal Facilities of the CBMSO and to Bloomington and Vienna stock centers for fly stocks. This work was supported by grants BFU2014-59438-P and BFU2017-83789-P and TENTACLES consortium RED2018-102411-T to IG from the Spanish Ministry of Science and Innovation and University and by institutional grants from the Fundación Areces and from Banco de Santander to the CBMSO. FPI fellowship from the Spanish Ministry of Science and Innovation and University supported A.A-T (BFU2014-59438-P).

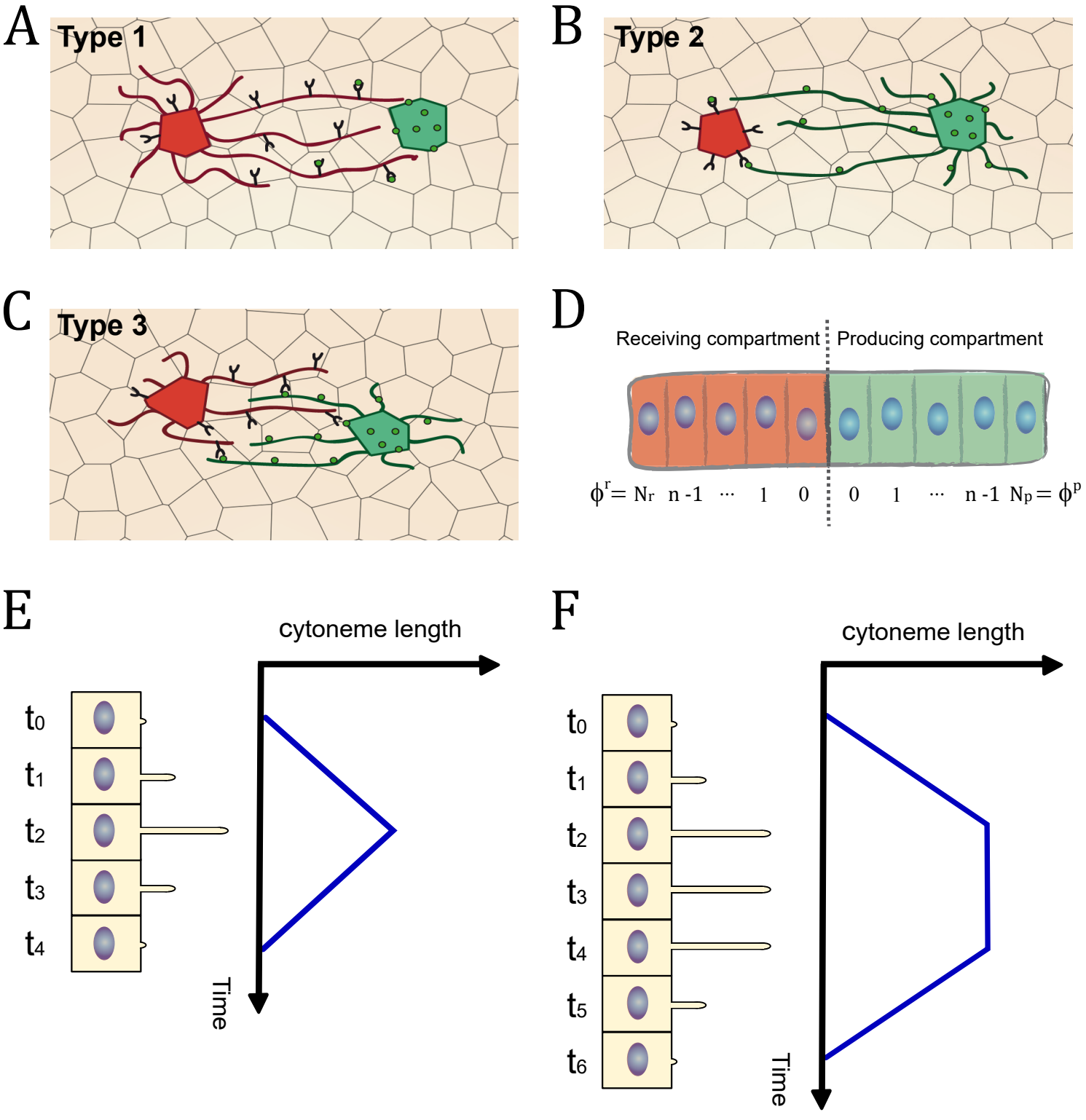
A
Type 1
B
Type 2
C
Type 3
D
Receiving compartment
Producing compartment
$\phi^r = N_r$ n -1 ··· 1 0 0 1 ··· n -1 $N_p = \phi^p$
E
cytoneme length
t_0
t_1
t_2
t_3
t_4
Time
F
cytoneme length
t_0
t_1
t_2
t_3
t_4
t_5
t_6
Time

Figure 1. Schemes of cytoneme-mediated cell signaling based on experimental evidence: A) Type 1: Receiving cells emit cytonemes to collect the morphogen from producing cells. B) Type 2: Producing cells emit cytonemes to deliver the morphogen to receiving cells. C) Type 3: Both producing and receiving cells emit cytonemes to deliver and collet the morphogen respectively. D) Frame of reference used to develop the mathematical equations. E) Schematic representation of the cytoneme triangular dynamics. F) Schematic representation of the cytoneme trapezoidal dynamics.

Inputs → *in silico* settings → Outputs

A

1 Experimental data

Gradient distribution	Cytoneme length	Time elongation	...	...
x1, y1	L1	te1	t1	t1
x2, y2	L2	te2	t2	t2
...	...	...	...	...
Xn, Yn	Ln	ten	tn	tn

2 GUI parameters

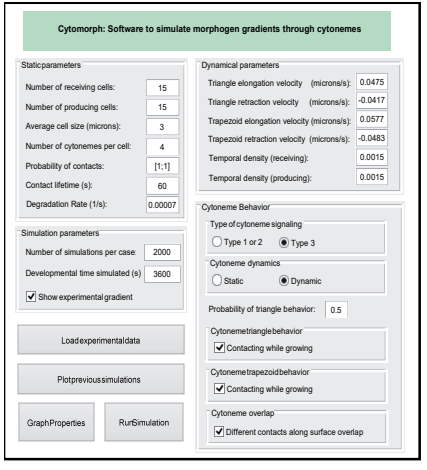

B

1

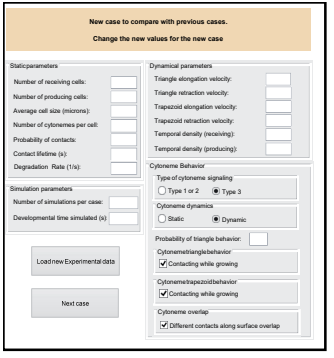

2

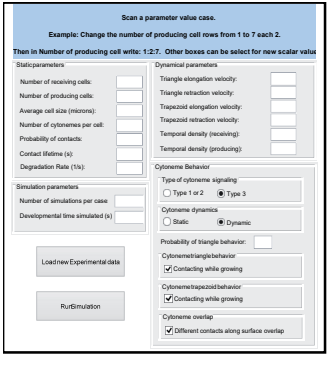

3

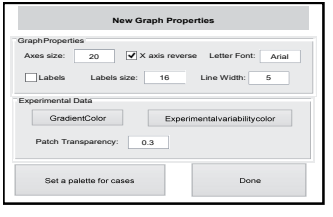

Comparison between cases

Variable role (Scan case)

Graph settings

C

1

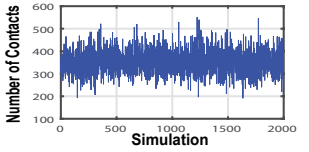

2

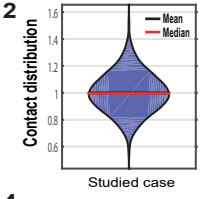

3

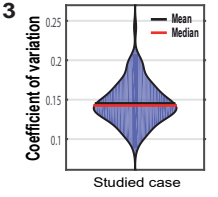

4

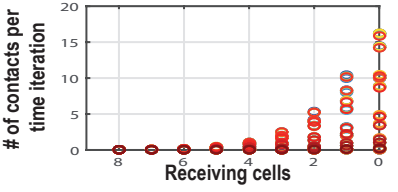

5

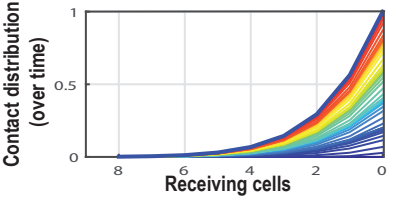

6

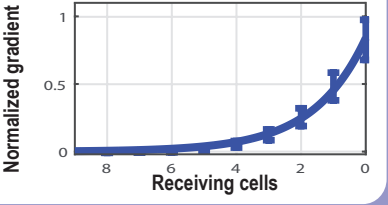

Figure 2. General outline of the Cytomorph workflow: A) Inputs of the Cytomorph, divided into two groups: A.1) Loading the data through an Excel table. A.2) Loading it through the main GUI. B) Cytomorph secondary GUI windows: B.1) Window in which different parameter combinations (cases) can be loaded to compare with the reference case. B.2) Window in which a scan of variable values can be selected to study their effect. B.3) Window in which graphical properties can be selected. C) Graphic outputs of Cytomorph simulations: C.1 and C.2) Contacts per cell along simulations. C.3) Signal variability measured by coefficient of variation. C.4) Contacts per cell and iteration. C.5) Temporal evolution of the contact distribution. C.6) Final gradient and expected variability (error bars).

A

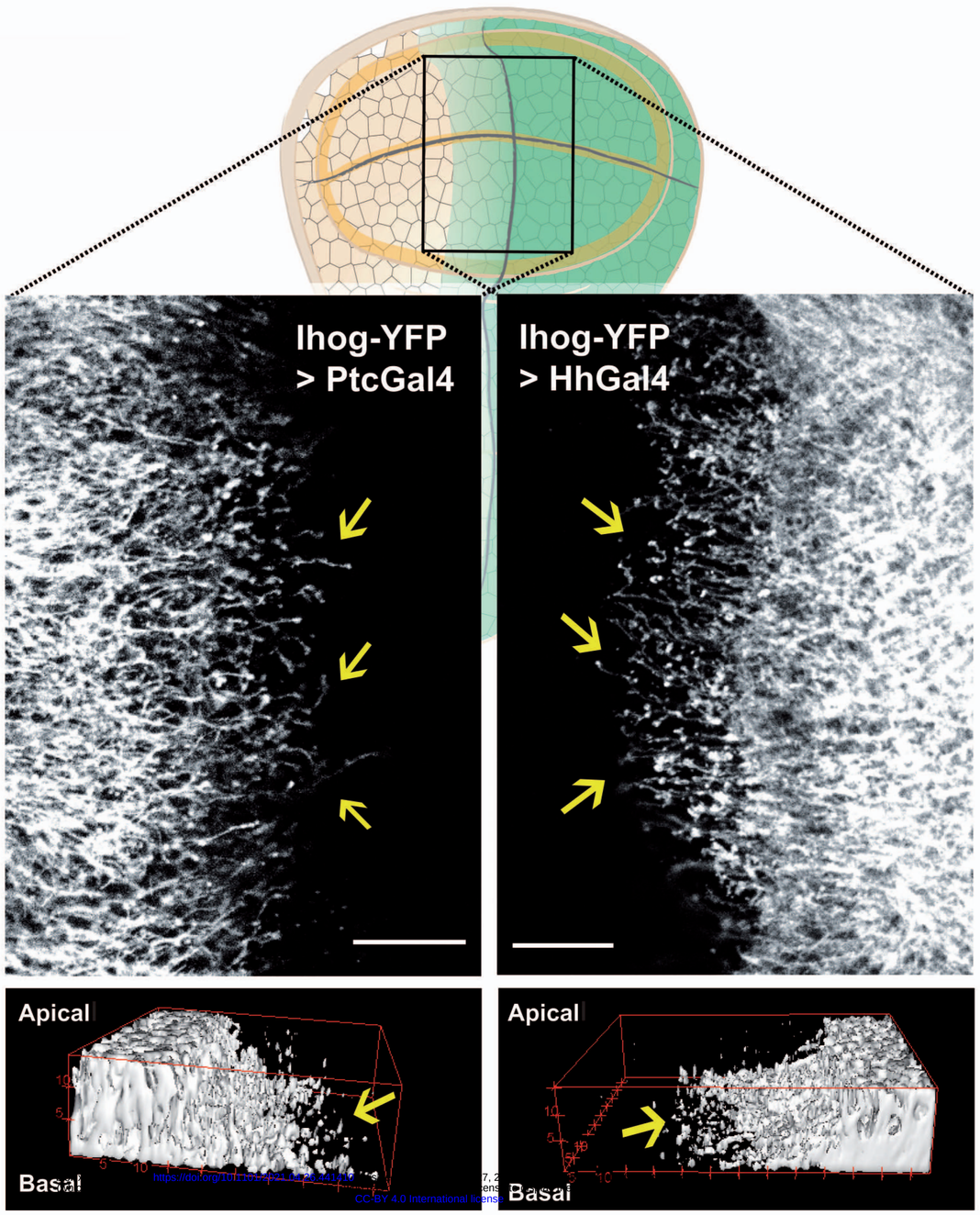
Ihog-YFP
> PtcGal4
Ihog-YFP
> HhGal4
Apical
Basal
Apical
Basal

B

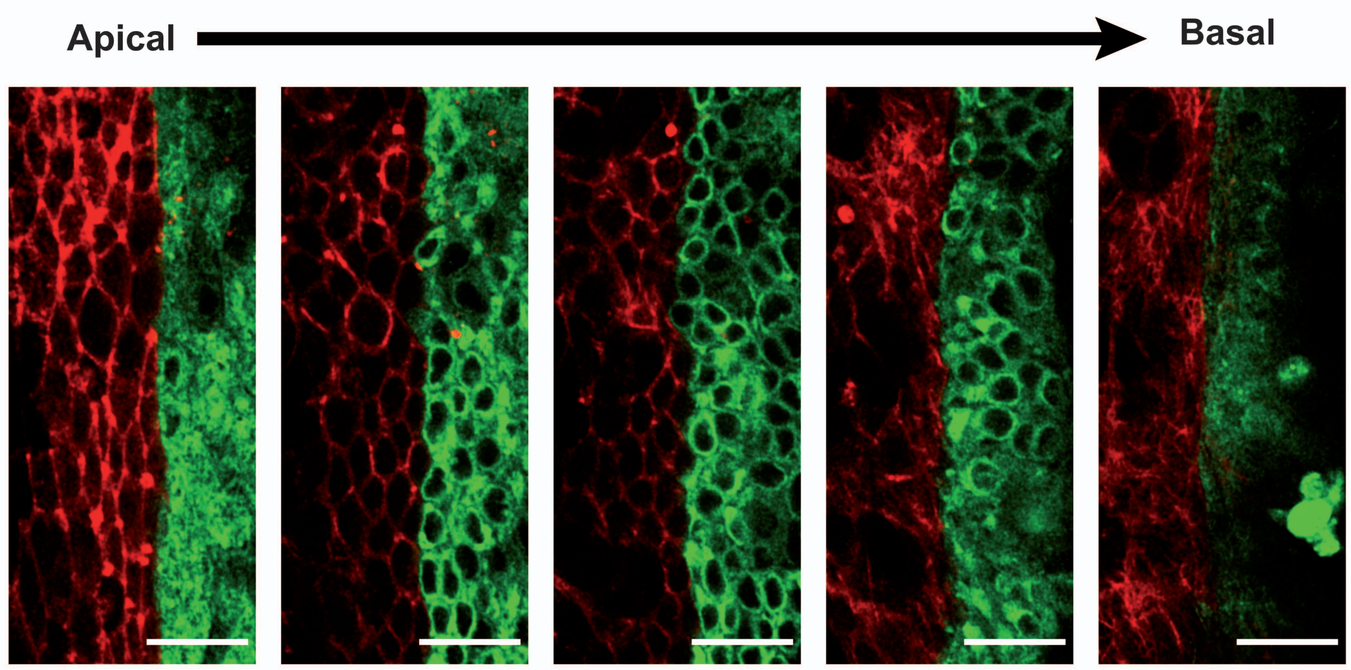
Apical
Basal

C

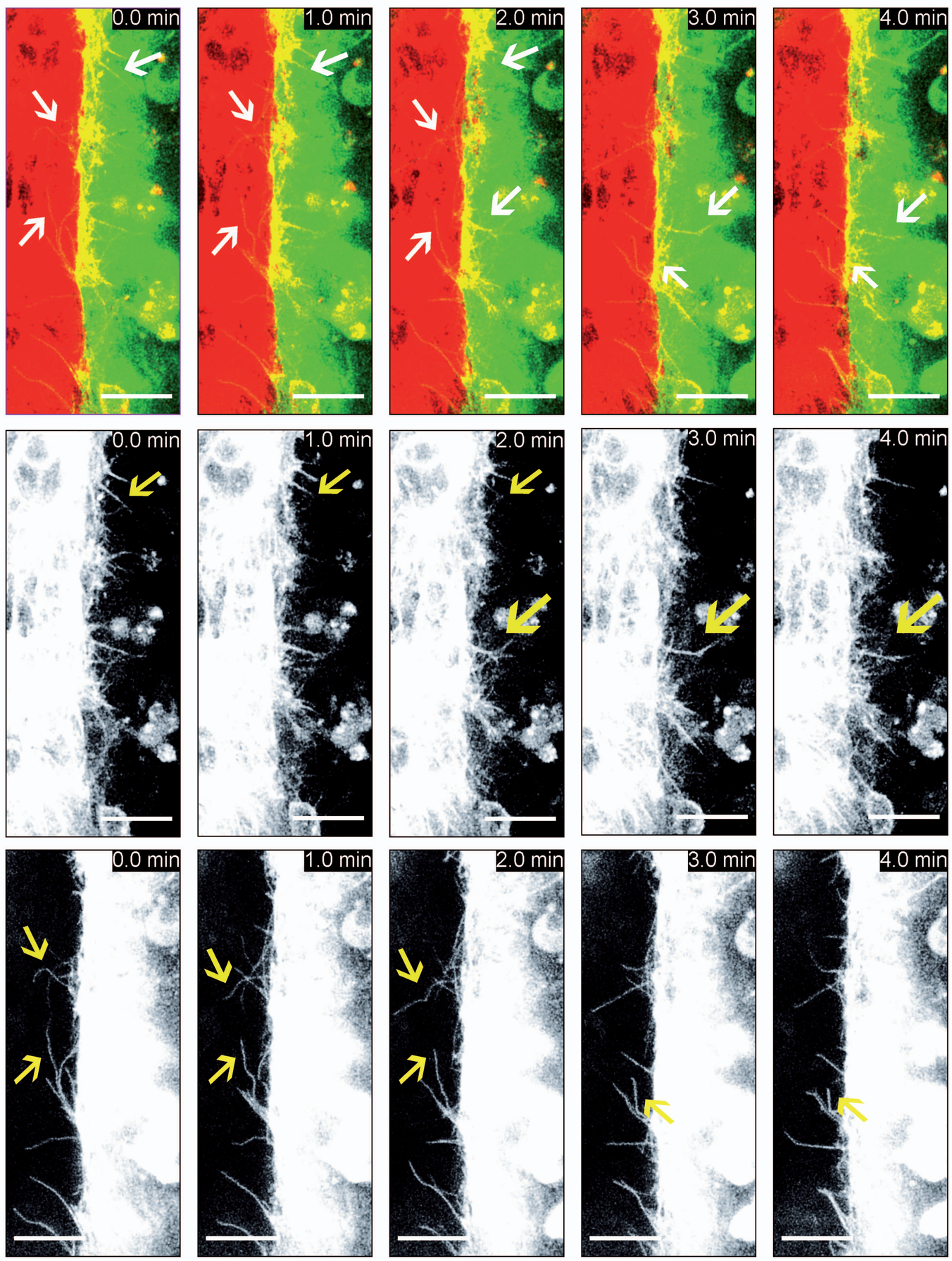
LifeActin-RFP > PtcGal4
mCD8-GFP > Hh QF
0.0 min
1.0 min
2.0 min
3.0 min
4.0 min
LifeActin-RFP > PtcGal4
mCD8-GFP > Hh QF

D

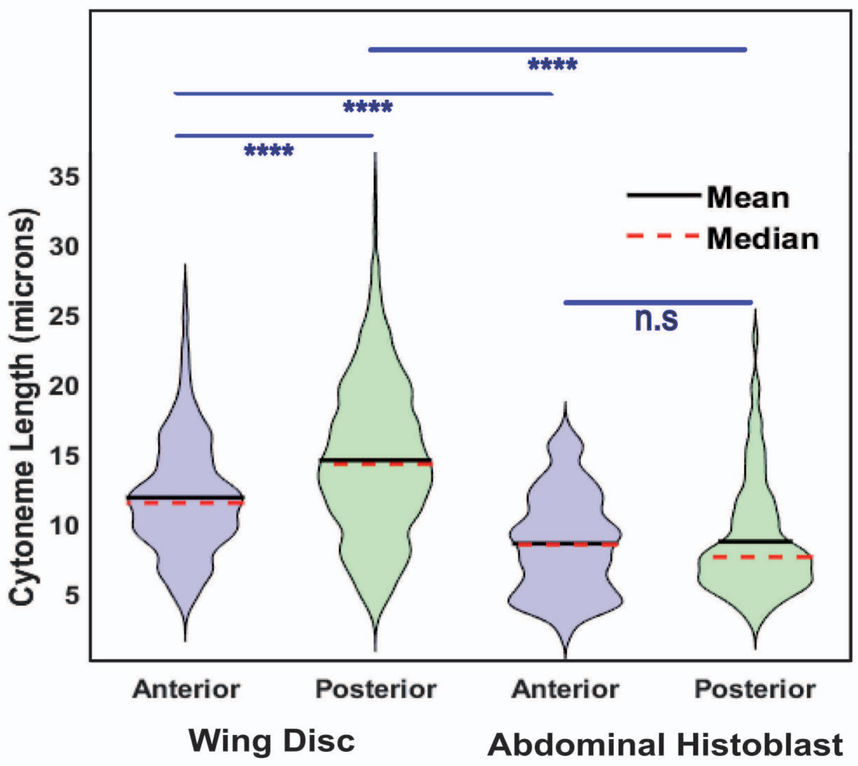
****
****
****
n.s
Mean
Median
Cytoneme Length (microns)
35
30
25
20
15
10
5
Anterior
Posterior
Anterior
Posterior
Wing Disc
Abdominal Histoblast

Figure 3. Experimental cytoneme characterization in *Drosophila* tissues. A) Wing imaginal disc cytonemes protruding from A (top left) and from P (top right) compartment cells marked with Ihog-RFP. Bottom panels show 3D reconstructions of a confocal Z-stack taken at the basal side of the tissue showing cytonemes protruding and from A (bottom left) and P (bottom right) compartment cells. B) A confocal Z-stack taken from the apical to basal side of the abdominal histoblast epithelium with the A compartment marked with life-actin-RFP (red) and the P compartment marked with CD8GFP (green). C) *In vivo* temporal sequence of abdominal histoblast cytonemes taken at one-minute intervals. Top image sequences show both A and P compartment labelled cytonemes (A in red, P in green), middle image sequences show a single channel of A compartment cytonemes, and bottom image sequences show the single channel of P compartment cytonemes. D) Statistical violin plots of cytoneme length distribution in the A (blue) and the P (green) compartments in wing disc (left) and abdominal histoblast nest (right). Scale bars: 15μm

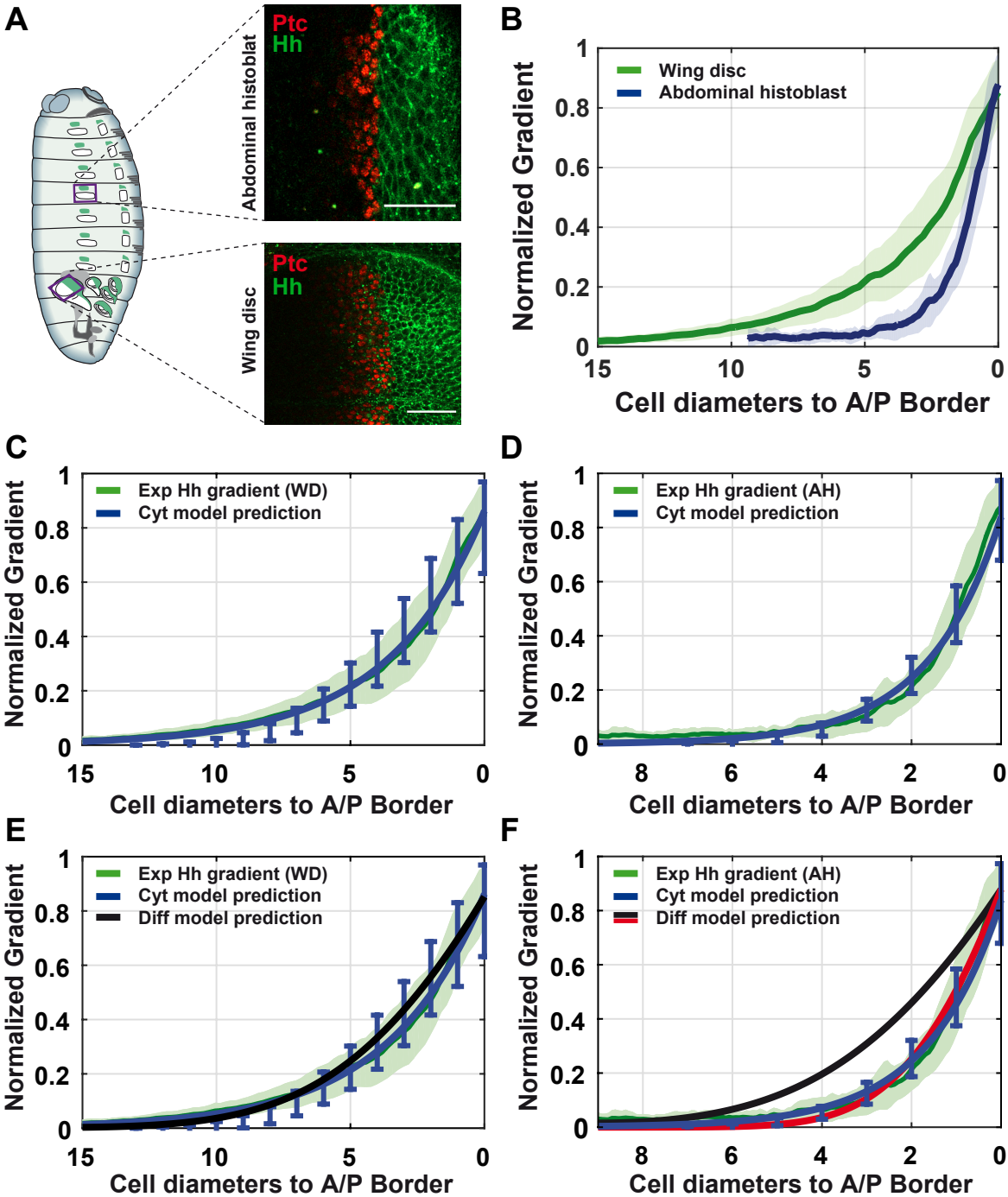
A
Ptc
Hh
Abdominal histoblat
Ptc
Hh
Wing disc
B
Wing disc
Abdominal histoblast
Normalized Gradient
Cell diameters to A/P Border
C
Exp Hh gradient (WD)
Cyt model prediction
Normalized Gradient
Cell diameters to A/P Border
D
Exp Hh gradient (AH)
Cyt model prediction
Normalized Gradient
Cell diameters to A/P Border
E
Exp Hh gradient (WD)
Cyt model prediction
Diff model prediction
Normalized Gradient
Cell diameters to A/P Border
F
Exp Hh gradient (AH)
Cyt model prediction
Diff model prediction
Normalized Gradient
Cell diameters to A/P Border

Figure 4. Experimental and simulated Hh gradients in *Drosophila* tissues. A) Confocal sections of *Drosophila* epithelia labeled with *Hh:GFP BAC* and *EnhancerPtcRed*. Top: abdominal histoblast nest. Bottom: imaginal wing disc. B) Quantified data of the Hh gradient in both epithelia: wing disc (green) and abdominal histoblast nest (blue). C) Comparison between the wing disc experimental gradient (green) and the predicted gradient estimated by our cytoneme model (blue). D) Comparison between the abdominal histoblast nest experimental gradient (green) and the predicted gradient estimated by cytoneme model (blue). E) Comparison between the wing disc experimental gradient (green) and the predicted gradients applying different models: cytoneme model (blue) and diffusion-degradation model (black). F) Comparison between the abdominal histoblast experimental gradient (green) and the predicted gradients applying different models: cytoneme model (blue) and diffusion-degradation model with different diffusion coefficient (red 3 times smaller than black). Scale bars: 30μm.

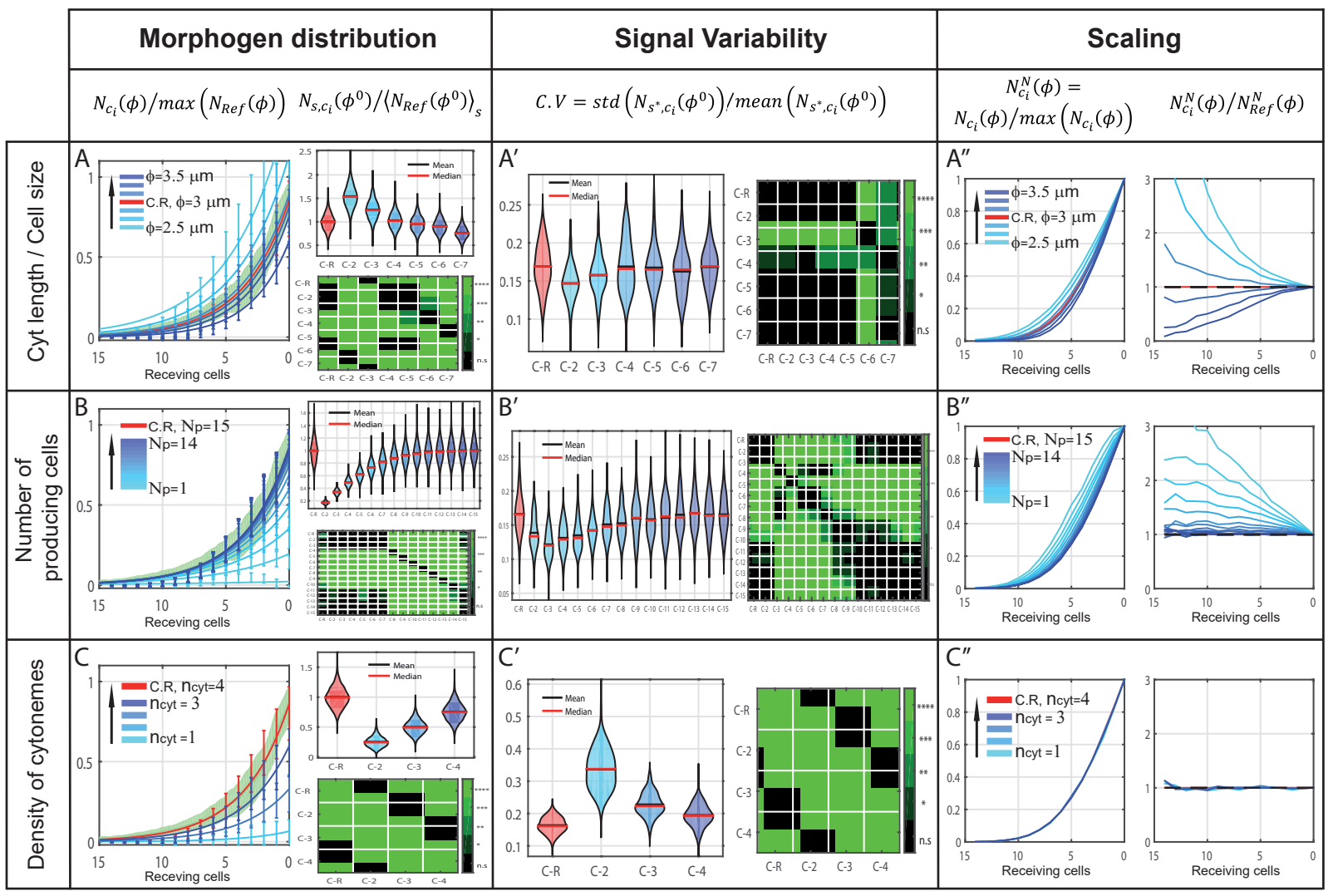
Morphogen distribution
Signal Variability
Scaling
$N_{c_i}(\phi)/max\left(N_{Ref}(\phi)\right)$
$N_{s,c_i}(\phi^0)/\langle N_{Ref}(\phi^0)\rangle_s$
$C.V = std\left(N_{s^*,c_i}(\phi^0)\right)/mean\left(N_{s^*,c_i}(\phi^0)\right)$
$N_{c_i}^N(\phi) = N_{c_i}(\phi)/max\left(N_{c_i}(\phi)\right)$
$N_{c_i}^N(\phi)/N_{Ref}^N(\phi)$
Cyt length / Cell size
Number of producing cells
Density of cytonemes
A
A′
A″
B
B′
B″
C
C′
C″
ϕ=3.5 μm
C.R, ϕ=3 μm
ϕ=2.5 μm
C.R, Np=15
Np=14
Np=1
C.R, ncyt=4
ncyt = 3
ncyt =1
Mean
Median
Receving cells
C-R C-2 C-3 C-4 C-5 C-6 C-7
n.s

Figure 5. ***In silico*** **study of different cytoneme variables and their predicted impact on gradient features.** Reference simulation in red, simulations after modifying a specific parameter in blue (graded light to dark depends on the value) and experimental data in green. X) Left. Morphogen distribution for different cases, normalized to the maximum value of the reference case, along receiving cells including the expected variability per cell row (error bars). Right. Study of the number of contacts in the first row of receiving cells ϕ^0, normalized to the average value of the reference case: top, violin plots of 2000 simulations per case; bottom, green-color-coded matrix of p-values for the violin distributions. X') Coefficient of variation per case in the first row of receiving cells ϕ^0 (left). Green-color-coded matrix of p-values for violin distributions (right). X'') Distribution of contacts normalized to their maximum value to compare changes in gradient shape along receiving cells (left). Coefficient of the normalized distributions to study the scaling along receiving cells (right). A) Simulations for different cell size/cytoneme length ratios (ϕ =2.5 to 3.5 each 0.2 μm (blue), ϕ=3 μm (red)). B) Simulations for different number of producing cells rows involved in the signaling (Np=1 to 14 (blue), Np=15 (red)). C) Simulations for different number of cytonemes per cell (n_{cyt}=1 to 3 (blue), n_{cyt}=4 (red)).

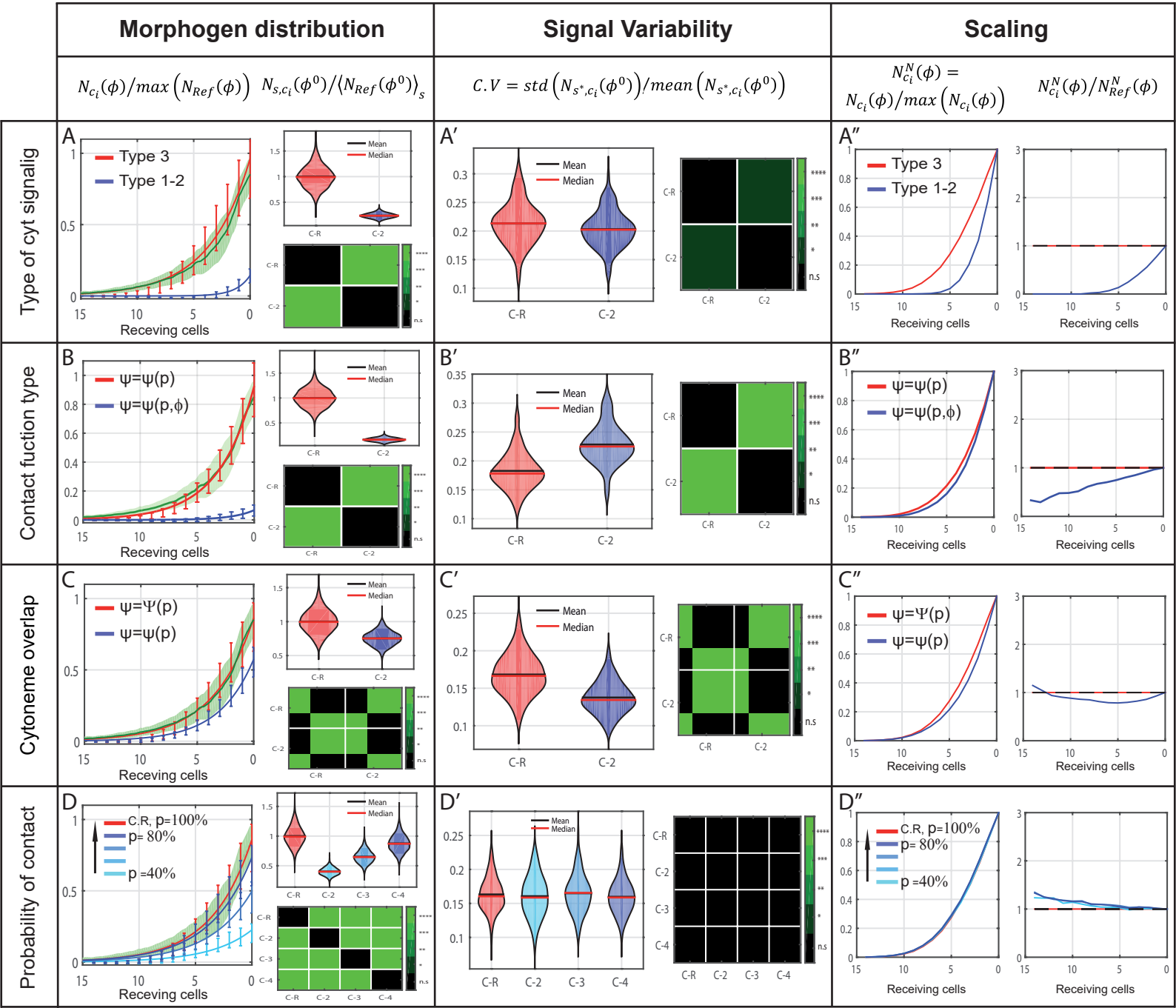
Morphogen distribution
Signal Variability
Scaling
$N_{c_i}(\phi)/max\left(N_{Ref}(\phi)\right)$
$N_{s,c_i}(\phi^0)/\langle N_{Ref}(\phi^0)\rangle_s$
$C.V = std\left(N_{s^*,c_i}(\phi^0)\right)/mean\left(N_{s^*,c_i}(\phi^0)\right)$
$N_{c_i}^N(\phi) = N_{c_i}(\phi)/max\left(N_{c_i}(\phi)\right)$
$N_{c_i}^N(\phi)/N_{Ref}^N(\phi)$
Type of cyt signalig
Contact fuction type
Cytoneme overlap
Probability of contact
A
A′
A″
B
B′
B″
C
C′
C″
D
D′
D″
Type 3
Type 1-2
ψ=ψ(p)
ψ=ψ(p,ϕ)
ψ=Ψ(p)
ψ=ψ(p)
C.R, p=100%
p= 80%
p =40%
Receving cells
Receiving cells
Mean
Median
C-R
C-2
C-3
C-4
n.s

Figure 6 *In silico* study of different cytoneme presumptions and their predicted impact on gradient features. Reference case in red, simulations after modifying a feature in blue and experimental data in green. X) Left. Morphogen distribution along receiving cells for different cases, normalized to the maximum value of the reference case, showing the expected variability per cell row (error bars). Right. Study of the number of contacts in the first row of receiving cells ϕ^0, normalized to the average value of the reference case. Top, violin plots of 2000 simulations per case. Bottom, green-color-coded matrix of p-values for the violin distributions. X') Coefficient of variation per case in the first row of receiving cells ϕ^0 (left). Green-color-coded matrix of p-values for violin distributions (right). X´´) Distribution of contacts normalized to their maximum value to compare changes in gradient shape along receiving cells (left). Coefficient of the normalized distributions to study the scaling along receiving cells (right). A) Simulations for different cytoneme signaling type (type 3 in red and type1-2 in blue). B) Simulations for different contact functions (type $\psi(p)$ in red and type $\psi(p,\phi)$ in blue). C) Simulations of the hypothetical case of multiple contacts between cytonemes along the overlapping surface (single contact in blue, multiple contacts in red). D) Simulations for different probability of contact (p=40% to 80% each 20% in blue, p=100% in red).

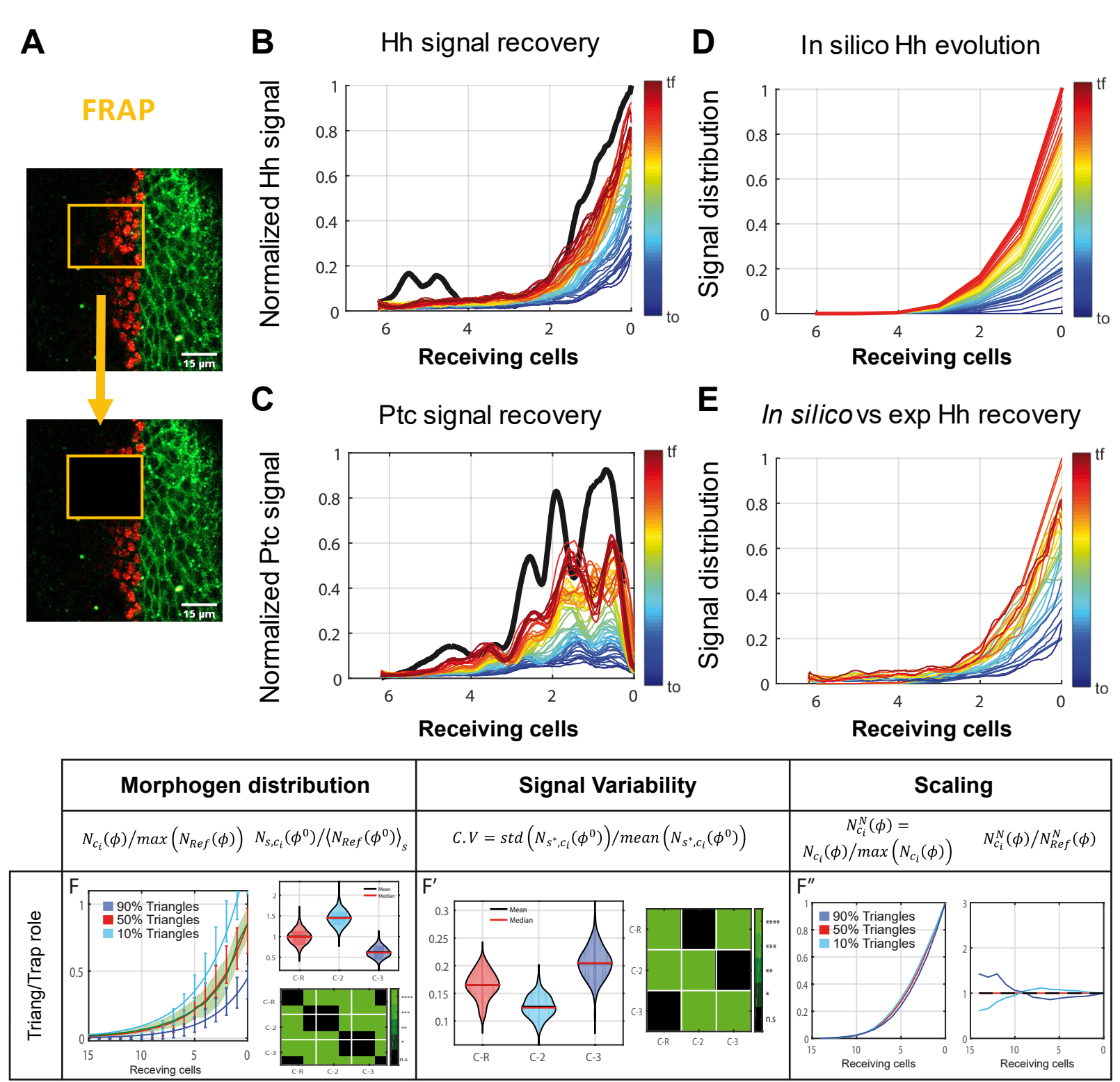
A
FRAP
15 µm
15 µm
B
Hh signal recovery
Normalized Hh signal
Receiving cells
tf
to
C
Ptc signal recovery
Normalized Ptc signal
Receiving cells
D
In silico Hh evolution
Signal distribution
Receiving cells
E
In silico vs exp Hh recovery
Signal distribution
Receiving cells
Morphogen distribution
Signal Variability
Scaling
$N_{c_i}(\phi)/max\left(N_{Ref}(\phi)\right)$
$N_{s,c_i}(\phi^0)/\langle N_{Ref}(\phi^0)\rangle_s$
$C.V = std\left(N_{s^*,c_i}(\phi^0)\right)/mean\left(N_{s^*,c_i}(\phi^0)\right)$
$N^N_{c_i}(\phi) = N_{c_i}(\phi)/max\left(N_{c_i}(\phi)\right)$
$N^N_{c_i}(\phi)/N^N_{Ref}(\phi)$
Triang/Trap role
F
90% Triangles
50% Triangles
10% Triangles
Receving cells
F′
Mean
Median
C-R
C-2
C-3
n.s
F″
90% Triangles
50% Triangles
10% Triangles
Receiving cells
Receiving cells

Figure 7. FRAP experiments to study the temporal gradient formation. A) Representative image of FRAP experiments in abdominal histoblast nests in which the signal is eliminated after photobleaching over a specific ROI. B) Hh (*Hh:GFP BAC*) gradient profile shortly before bleaching in black and Hh signal recovery over time coded in a hot colormap; each step corresponds to 45 seconds. C) *Ptc* (*EnhancerPtcRed*) expression profile shortly before bleaching in black and *ptc* signal recovery over time coded in a hot colormap, each step is 45 seconds. D) *In silico* signal evolution predicted for abdominal histoblast nests. E) A graphical comparison every 3 minutes between *in silico* simulations and experimental data. F) Simulations for cytonemes contacting while growing with a different ratio of triangular/trapezoidal cytoneme dynamics (10% triangles in light blue, 50% triangles in red, 90% triangles in dark blue). Scale bars: 15μm.